journal

J. Am. Ceram. Soc., **81** [10] 2549–57 (1998)

Optical Properties of Aluminum Oxide: Determined from Vacuum Ultraviolet and Electron Energy-Loss Spectroscopies

Roger H. French*,† Harald Müllejans,‡,§ and David J. Jones†

E. I. du Pont de Nemours and Company, Wilmington, Delaware 19880; and
Max-Planck-Institut für Metallforschung, D-70174 Stuttgart, Germany

The optical properties of α-Al_2O_3 have been determined by two independent methods, vacuum ultraviolet (VUV) spectroscopy and electron energy-loss spectroscopy (EELS) over the energy range from 6 to 142 eV. For each experimental method two sets of high-quality data have been measured and analyzed from α-Al_2O_3. The evolution of the differences between the data for each experimental method and its associated analytical method indicate the reliability of the results, and the comparison between the methods emphasizes the relative advantages of each. VUV spectroscopy offers a higher energy resolution, resolving sharper features in the spectra, whereas EELS significantly extends the energy range, which has been exploited here to 140 eV but can be extended even further. Good overall consistency is found, but there are pronounced differences in the valence region from 10 to 30 eV, where strong absorptions are present, increasing the relative variability of the analysis. This demonstrates that accuracy estimates of the optical properties are meaningful only when supplied as a function of energy, because both strong intrinsic absorptions and weak experimental signals make accurate determinations difficult. Moreover, variations in the optical properties are observed most easily in the interband transition strength, J_{cv}, and are less evident when the optical properties are represented as the complex index of refraction. Because the optical properties can change with specimen origin and preparation and because of the details of data acquisition and numerical analysis procedures, assessing the contributions of each of these methods to our accurate knowledge of the optical constants is essential.

I. Introduction

ALUMINA (Al_2O_3) has a variety of applications as a structural ceramic and as an optical material, for example, in sodium-vapor arc lamps and in thin-film devices. The latter applications make use of the electronic structure and bonding present in Al_2O_3. For an understanding and improvement of the material in these applications, the optical constants of Al_2O_3[1–4] have to be known with high accuracy. Optical properties also are required for dispersion-force and Hamaker constant determinations using the full spectral method,[5–7] and they also are important for Hamaker constant determination from atomic force microscopy (AFM) force–distance curves.[8] In the past, the optical properties and the electronic structure of α-Al_2O_3 have been determined from vacuum ultraviolet (VUV) reflectance spectroscopy at room temperature[9] and high temperatures,[10,11] up to the melting point.[12] Further measurements with synchrotron radiation at room temperature and low temperature (10 K) have been reported by Tomiki *et al.*[13,14] There also have been critiques of the optical constants of Al_2O_3 that have reviewed the literature to date,[15] and a new critique has been published recently.[16]

Crystal defects, such as grain boundaries and interfaces also are critical in applications of Al_2O_3 and influence its macroscopic properties. Therefore, the interfacial electronic structure and bonding of a Σ11 grain boundary in α-Al_2O_3 has been studied in detail by valence electron energy-loss spectroscopy (EELS).[17] This has been complemented by calculation in the local density approximation of the band structure[18] and the optical constants.[19] These studies always have compared the interfacial properties to the bulk properties, as determined by the identical experimental technique. Thereby, it has been possible to detect differences between bulk and interface and to semiquantitatively determine the changes in the interfacial electronic structure. In many applications such as these, the *absolute* bulk optical properties serve as a starting point. In this article, we present the determination of the optical constants of α-Al_2O_3 by two independent methods, VUV spectroscopy and EELS, using the currently best analysis routines, developed during the work on grain boundaries.[17] For each method, two sets of measurements have been taken and fully analyzed. The accuracy and reliability of each method is thereby revealed. A comparison of both methods shows their respective advantages. We also present the optical constants from γ-Al_2O_3 and δ-Al_2O_3, determined by EELS.

II. Experimental Techniques

(1) Specimen Preparation

The specimens studied for VUV spectroscopy were single crystals of α-Al_2O_3, whereas polycrystalline Al_2O_3 films were studied in EELS. Even with these specimen differences, the optical constants of α-Al_2O_3 were comparable.

(A) For VUV Spectroscopy: The specimens used for VUV spectroscopy were basal-plane, UV-grade, single-crystals of undoped α-Al_2O_3, supplied with an Epi-Grade chemical–mechanical polish (Crystal Products Division, Union Carbide Co., Washougal, WA). These UV-grade samples had high surface quality with low dislocation density. One specimen was measured as-received, whereas the other was laser heated to 1040°C under vacuum for 3 h prior to the measurement; details have been reported previously.[12]

(B) For EELS: Polycrystalline Al_2O_3 films, containing α, γ, and δ phases, were investigated by EELS. The material and transmission electron microscopy (TEM) specimen preparation have been described fully elsewhere.[20] Briefly, thin films of amorphous Al_2O_3 were prepared by anodization of 99.999% aluminum foil in a 0.01*M* aqueous solution of ammonium tartrate ($(NH_4)_2C_4H_4O_6$) at room temperature. Free-standing Al_2O_3 films were produced after anodization was completed by

W. C. LaCourse—contributing editor

Manuscript No. 191076. Received April 15, 1997; approved February 2, 1998.
*Member, American Ceramic Society.
†E. I. du Pont de Nemours.
‡Max-Planck-Institut für Metallforschung.
§Now at the Institute for Advanced Materials, Joint Research Centre, EC, 1755 ZG Petten, The Netherlands.

etching away the remaining aluminum in 2% mercuric chloride ($HgCl_2$) solution and retrieving the floating films on an Al_2O_3 TEM support. Films prepared by this route were placed in a pure Al_2O_3 crucible and annealed in air for 15 min at 1200°C. The TEM specimen was coated with carbon to avoid charging during investigation by electron microscopy.

The specimen contained α-, γ- and δ-Al_2O_3. γ-Al_2O_3 has been described as a defect spinel structure, with the vacant cation sites randomly distributed, whereas δ-Al_2O_3 is closely related to γ-Al_2O_3, being viewed as a superstructure of γ-Al_2O_3.[20] δ-Al_2O_3 can be distinguished from γ-Al_2O_3 by the presence of superlattice reflections and by the absence of certain other reflections. However, two sections (in [001]γ and [110]γ) are required to establish the presence of δ-Al_2O_3 unambiguously. This has not been possible for this specimen; therefore, there remains an uncertainty whether actually both γ- and δ-Al_2O_3 are present, or just one of them.

For consistency, specimens of plasma-sprayed Al_2O_3 coatings on ZnO containing α- and δ-Al_2O_3 also were measured. The material was provided by K. Rajan (Rensselaer Polytechnic Institute, Troy, NY), and energy-dispersive X-ray spectroscopy (EDS) analysis revealed no impurities. The specimens were annealed further at 1100°C in air for 1 h. The TEM specimens were prepared by polishing to a thickness of 30 μm, followed by dimpling and ion thinning in a precision ion-polishing system (Model PIPS, Gatan, Pleasanton, CA).

(2) Optical Spectroscopy

(A) VUV Spectroscopy: VUV spectroscopy has become an established technique for electronic structure studies of large-band-gap, insulating ceramics. It has the advantage of covering the complete energy range of the valence interband transitions.[21] The VUV spectrophotometer, the details of which have been discussed previously,[22] utilizes a laser plasma light source (LPLS)[23] and iridium reference mirrors. The energy range of the instrument is from 1.7 to 44 eV, or from 700 to 28 nm, which extends beyond the air cutoff of 6 eV and the window cutoff of 10 eV. The resolution of the instrument is 0.2–0.6 nm, which corresponds to 16 meV resolution at 10 eV and 200 meV resolution at 35 eV. The VUV spectrophotometer utilizes unpolarized light, so that the only polarization-dependent results result from comparison of single-crystal specimens prepared so that the *c*-axis is normal to the specimen surface (basal plane) or is in the plane of the specimen surface. In the present work, basal-plane specimens of α-Al_2O_3 are used, and polarization dependence of the optical constants has not been determined. The use of synchrotron radiation sources in VUV spectroscopy allows full-polarization-dependent studies, because these light sources, as opposed to the LPLS, are polarized.

(B) Ultraviolet/Visible: The measurements from 0.4 to 6 eV were taken using a UV–visible–near infrared (NIR) spectrophotometer (Model Lambda 19, Perkin-Elmer Corp., Norwalk, CT) with an absolute reflectance attachment of the V-W type. For the reflectance of these specimens in the W configuration, the first reflected bounce was from the specimen, whereas an aluminum reference mirror was used for the second bounce. The results were corrected for this reference mirror reflectance to determine the reflectance of the specimen. Transmission was measured over the complete energy range of the instrument for use in the second-surface reflectance correction. The wavelength (energy) resolution was 2 nm (40 meV) at 5.0 eV. The results agreed well with the data from the VUV and NIR spectrophotometers, and data were spliced together in the overlapping energy regions without the need to use a multiplicative scaling factor.

(3) EELS

EELS is a valuable tool for investigating various aspects of materials.[24] It has the advantage of covering the complete energy range, including valence interband transitions and core level excitations. When performed with TEM, it has a spatial resolution in the nanometer range, which allows the selection of small features within a specimen.

The EELS measurements were performed with a parallel electron energy-loss spectrometer (PEELS, Model 666, Gatan) fitted to a dedicated scanning transmission electron microscope (STEM, Model HB501, Vacuum Generators, Perkin-Elmer Corp., Norwalk, CT) operating at 100 keV. The system had an energy resolution of 0.9 eV, determined by the full-width half-maximum of the zero-loss peak. The beam diameter was <1 nm, and spectra were acquired while the beam was scanning an area of 6 nm × 8 nm. The convergence and collection semi-angle were 10 and 13 mrad, respectively. The visual inspection of the image before, during, and after data acquisition showed no sign of electron-beam irradiation damage of the specimen. The energy dispersion was 0.1 eV, which corresponded to 100 eV width of the spectrum. For each measurement, two spectra (for 10 s each) were acquired, one covering the energy range −10 to 90 eV and the other 40 to 140 eV. Each spectrum was corrected for dark current and readout pattern (measured under identical conditions as the spectra themselves but with the primary electron-beam switched off) and the channel-to-channel gain variation (determined by flat-field illumination of the photodiode array). The two spectra then were spliced together to give one continuous spectrum in the energy-loss range of −10 to 140 eV.

Four measurements were taken from the polycrystalline Al_2O_3 sample prepared from anodic Al_2O_3 films, two from α-Al_2O_3 and one each from γ- and δ-Al_2O_3. These data are presented in the remainder of this paper. For consistency, data were acquired from the α and δ phases in the plasma-sprayed Al_2O_3 specimen. The EELS results were consistent within the variation of the method, as discussed below, and, therefore, these data were not analyzed further.

The specimen thickness was determined from the absolute intensity of the EELS oxygen *K* edge and the sum rule for the low loss[24] (Sections III(2) and III(3)(B)). Both methods gave, for all three areas, thicknesses of ~40 nm with a repeatability of ±5 nm. The thickness of the carbon coating layer was calculated from the carbon *K* edge and found to be 5 nm.

III. Analytical Methods

This section describes the data analysis required to transform the experimentally measured data into the complex optical properties. This consists of the rather complex and sensitive integral transforms that form the basis of Kramers–Kronig (KK) dispersion analysis,[25,26] which is followed by the usual algebraic transformations of any one complex optical property to any other. Once this is achieved, i.e., the data of various methods and measurements are on a common basis, a meaningful comparison of the reliability and information content is possible. We compare the results of the measurements and methods in various forms (Section IV). Most of the analytical details are discussed elsewhere for both the VUV spectroscopy[27] and EELS[28] data and are summarized only for completeness here.

(1) Optical Property Relations

The reflectance, *R*, measured by VUV spectroscopy is related to the index of refraction, *n*, according to

$$R(E) = \frac{(n-1)^2 + k^2}{(n+1)^2 + k^2} \tag{1}$$

where *E* is the energy and *k* the extinction coefficient. The complex index of refraction, $n + ik$, is related to the complex dielectric constant, ε,

$$\varepsilon_1 + i\varepsilon_2 = (n + ik)^2 \tag{2}$$

Likewise, there is a relation between the dielectric function and the energy-loss function, ELF:

$$\mathrm{ELF}(E) = \mathrm{Im}\left(\frac{-1}{\varepsilon(E)}\right) = \frac{\varepsilon_2}{\varepsilon_1^2 + \varepsilon_2^2} \tag{3}$$

where Im indicates imaginary part. ELF represents the response of a material to fast electrons traveling through it, as occurs in a TEM–EELS measurement.

(2) Single-Scattering Deconvolution of EELS

An expression for the single-scattering distribution, $S(E)$, for scattering with an energy-loss E and recorded for all scattering angles up to the collection angle, β, can be calculated with the help of dielectric theory:[29]

$$S(E) = \frac{I_0 t}{\pi a_0 m_0 v^2} \mathrm{Im}\left(\frac{-1}{\varepsilon(E)}\right) \ln\left[1 + \left(\frac{\beta}{\theta_E}\right)^2\right] \tag{4}$$

where I_0 is the intensity of the unscattered or elastically scattered electrons, t the thickness of the specimen, a_0 the Bohr radius, m_0 the electron mass, v the velocity of the incident electrons, and θ_E the characteristic scattering angle for inelastic scattering with energy-loss E. Equation (4) assumes the dipole approximation, i.e., $\varepsilon(E,\mathbf{q}) = \varepsilon(E,0) = \varepsilon(E)$ for small values of the momentum transfer $\mathbf{q}$, which is valid here.

The single-scattering spectrum is obtained from the recorded EELS spectrum by removing the zero-loss peak (zero-order scattering) and the multiple scattering (double- and higher-order scattering). Both are achieved with a Fourier–logarithmic deconvolution method[24] developed during this work.[28] A Lorentzian, or other analytical lineshape, is fitted to the experimental spectrum in the band-gap region (7–8 eV) and extended to the end of the recorded data. The zero-loss peak used for deconvolution consists of the recorded data up to 8 eV and the analytical shape for higher energies.[27] The spectra have been extended to 1000 eV by adding a high-energy wing following the power law E^{-4}.

(3) KK Dispersion Analysis

Because all optical properties are complex and only one part is measured, KK dispersion analysis[25] is used to determine the complex conjugate variable. The KK transform results from the KK dispersion relations, which are direct results of the physical principle of causality. Because the KK dispersion relation is formally correct only when the values of one variable of a conjugate pair are known at all energies from $E = 0$ to $E = \infty$, we approximate the infinite energy range by adding analytical extensions, or wings. We use a fast-Fourier-transform- (FFT-) based program (Electronic Structure Tools, Spectrum Squared, Ithaca, NY) running under GRAMS/32 (Galactic Industries, Salem, NH) to perform the KK transform integrals to speed the analysis and increase its accuracy.

(A) KK Analysis of Reflectance: Once the reflectivity of the sample is determined over a wide energy range, encompassing the interband transitions of the electrons, the KK dispersion relations for the reflectance[30] can be used to calculate the reflected phase, ϕ, of the light from the reflectance amplitude, ρ:

$$\phi(E) = -\frac{2E}{\pi} P \int_0^\infty \frac{\ln \rho(E')}{E'^2 - E^2}\, \mathrm{d}E' \tag{5}$$

where $\hat{R} = R + i\phi$ is the definition of the complex reflectance and $\rho = R^{1/2}$. The experimental reflectance data, consisting of data taken using the VUV and UV/visible spectrophotometers is extrapolated down to 0 eV on the low-energy (low-frequency) side. This is done using optical constants for Al_2O_3 determined from spectroscopic ellipsometry, or, in this case, from the literature,[15] to calculate the reflectance in the visible and then fitting a Sellmeier-type wing[31] simultaneously to the VUV and UV/visible data and the ellipsometric data in a chi-squared sense. On the high-energy side of the experimental data, the electrons behave essentially as free particles. Using the Lorenz–Oscillator model, it can be shown that the reflectance obeys a E^{-4} power law in this case.[32] Therefore, the reflectance is extended up to 1000 eV by a wing of the form AE^{-4}. The prefactor A is obtained by a fitting routine. Upon determination of the reflected phase, Eq. (6) can then be used to obtain the complex index of refraction and all other related optical properties:

$$\frac{n - 1 + ik}{n + 1 + ik} = \rho(E)\exp(i\theta(E)) \tag{6}$$

(B) KK Dispersion Analysis of EELS: The KK dispersion relations can be formulated for the energy-loss function as

$$\mathrm{Re}\left(\frac{1}{\varepsilon(E)}\right) = 1 - \frac{2}{\pi} P \int_0^\infty \mathrm{Im}\left(\frac{-1}{\varepsilon(E')}\right) \frac{E'}{E'^2 - E^2}\, \mathrm{d}E' \tag{7}$$

where Re indicates real part and P is the Cauchy principal part of the integral. No further wings have been added to the data because the high-energy wing already has been added for the single-scattering deconvolution. At the low-energy side, the data are truncated at 4 eV to avoid artifacts from spurious intensity in the band-gap region.

For $E = 0$ in Eq. (7), $\mathrm{Re}(1/\varepsilon) \approx 1/n^2$, where n is the refractive index for visible light, and

$$1 - \frac{1}{n^2} = \frac{2}{\pi} P \int_0^\infty \mathrm{Im}\left(\frac{-1}{\varepsilon(E')}\right) \frac{1}{E'}\, \mathrm{d}E' \tag{8}$$

Equation (8) is used to calculate the specimen thickness and the prefactor in Eq. (4) to transform the arbitrary scale of the EELS spectrum to an absolute scale of the energy-loss function. The refractive index is taken as 1.76 for α-Al_2O_3 and as 1.70 for γ- and δ-Al_2O_3.[33]

(4) Interband Transition Strength

The product of the joint density of states, J'_{cv}, and the square of the matrix element $|\mathbf{a}_0 \cdot \mathbf{p}_{ij}|$ is the interband transition strength $J_{cv}(E)$ and accounts for the dipole selection rules for the transitions. $J_{cv}(E)$ is proportional to the probability that a transition of an electron between the filled valence band and the empty conduction band with the transition energy E takes place and is related to $\varepsilon(E)$ by[27]

$$J_{cv}(E) = |\mathbf{a}_0 \cdot \mathbf{p}_{ij}|^2 J'_{cv}(E) = \frac{m_0^2 E^2}{e^2 \hbar^2 8\pi^2} (\varepsilon_2(E) + i\varepsilon_1(E)) \tag{9}$$

where e is the charge of the electron and $\hbar$ is Planck's constant. The imaginary part of $J_{cv}(E)$ results from dispersive processes. The interband transition strength $J_{cv}(E)$ has units of $\mathrm{g \cdot cm^{-3}}$. For computational convenience, we take the prefactor $m_0^2 e^{-2} \hbar^{-2}$ in Eq. (7), whose value is 8.289×10^{-6} $\mathrm{g \cdot eV^{-2}}$ as unity. Therefore, the $J_{cv}(E)$ spectra plotted in this paper have units of $\mathrm{eV^2}$.

(5) Oscillator Strength Sum Rule

From the KK dispersion relations, the oscillator strength sum rule can be formulated[34] for the interband transition strength $J_{cv}(E)$. $n_{eff}(E)$ is the number of electrons contributing to a transition up to an energy E:

$$n_{eff}(E) = \frac{4V_f}{m_0} \int_0^E \frac{J_{cv}(E')}{E'}\, \mathrm{d}E' \tag{10}$$

where V_f is the volume of one formula unit. The values of the formula unit volumes used in the present work are given in Table I.

IV. Results

(1) Reflectance

The reflectances measured of α-Al_2O_3 (Fig. 1) for the two specimens, one as-received and one annealed, show close agreement in all shapes and only minor differences in absolute

Table I. Al_2O_3 Formula-Unit Volumes Used for Oscillator Strength Sum Rule and Refractive Indexes Used for Sum Rule Calculations†

Phase	Al_2O_3 formula-unit volumes (nm^3)	Refractive index
α-Al_2O_3	0.0425	1.76
γ-Al_2O_3	0.0475	1.70
δ-Al_2O_3	0.0475	1.70

†Reference 33.

scale. The most pronounced difference is the feature at 9 eV, which appears sharper for the annealed sample.

The real and imaginary parts of the interband transition strength (Eq. (9)) have pronounced differences in the absolute intensity (Fig. 2). For the real part, $\mathrm{Re}[J_{cv}]$, these differences amount to two absolute units for all energies >12 eV. The excitonic peak at 9 eV is resolved clearly for the annealed sample, and it appears as a shoulder for the untreated material. For the imaginary part, $\mathrm{Im}[J_{cv}]$, the main differences appear for energies <12 eV.

The complex index of refraction (Fig. 3) exhibits differences similar to those described for the interband transition strength, but the index of refraction is a much less sensitive optical property in which to observe these variations.

(2) EELS

The dark and gain-corrected spliced spectra for α-Al_2O_3 appear on a different absolute scale, because the intensity has arbitrary units that depend on experimental parameters (Fig. 4). After correction for multiple scattering (Section III(2)), including the index sum rule scaling (Section III(3)(B)), the intensities of the energy-loss functions for both data sets agree closely (Fig. 5). The multiple-scattering correction is largest in the energy range 40–60 eV, where the twofold plasmon scattering occurs. Overall, the corrections are rather small, because the specimen thickness is only 0.4 times the total mean free path for inelastic scattering. After KK analysis, the interband transition strength is calculated (Figs. 2 and 6). There are small differences in intensity over the entire energy range from 0 to 140 eV, but it is most pronounced between 10 and 20 eV. Also, there is a small shift of the leading edge (Fig. 2(A)), possibly indicating a difference in the band-gap energy. The strong features at 78 eV and above result mainly from the excitation of aluminum $L_{2,3}$-shell electrons. Actually $\mathrm{Re}[J_{CV}] \propto \varepsilon_2 E^2$ (Eq. (9)) and, therefore, has the same appearance as the energy-loss function (although not visible in Fig. 5 because of the scale), because, in this energy-loss range, $\varepsilon_1 \approx 1$, and ε_2 is small, so that $\mathrm{Im}[-1/\varepsilon] \propto \varepsilon_2$ (Eq. (3)). The differences in the complex index of refraction (Fig. 7) also are apparent only for energies in the range 10–20 eV.

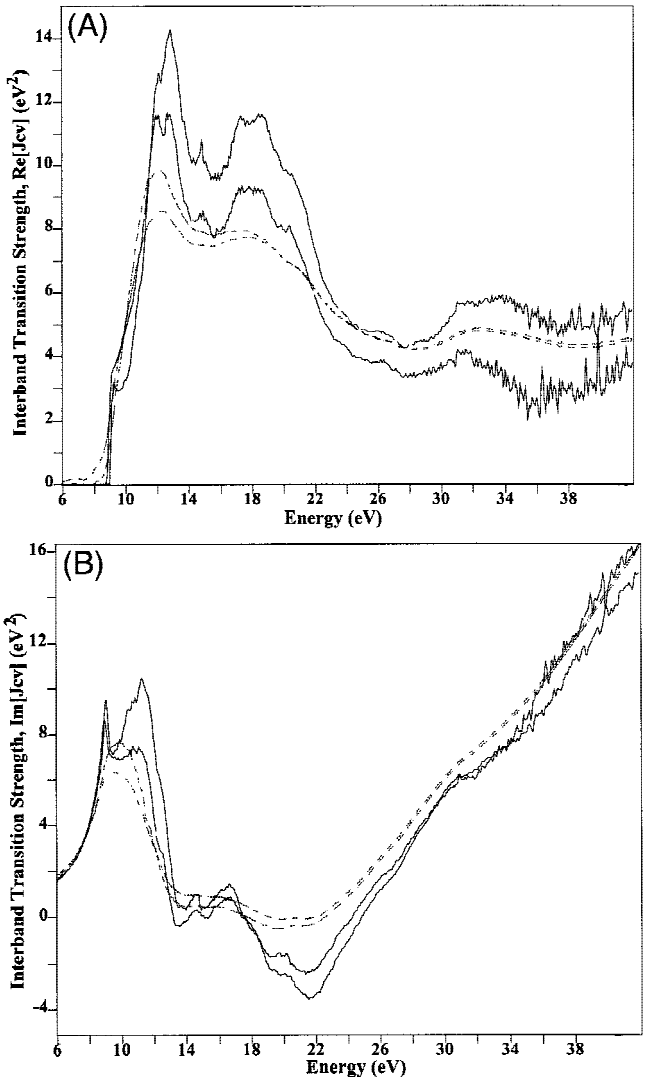

Fig. 2. Interband transition strength: (A) $\mathrm{Re}(J_{cv})$ and (B) $\mathrm{Im}(J_{cv})$ of single-crystal α-Al_2O_3, for E perpendicular to the c-axis, determined by KK analysis of VUV and UV/visible reflectance data. For comparison, the results from KK analysis of EELS data of α-Al_2O_3 also are shown (dashed lines).

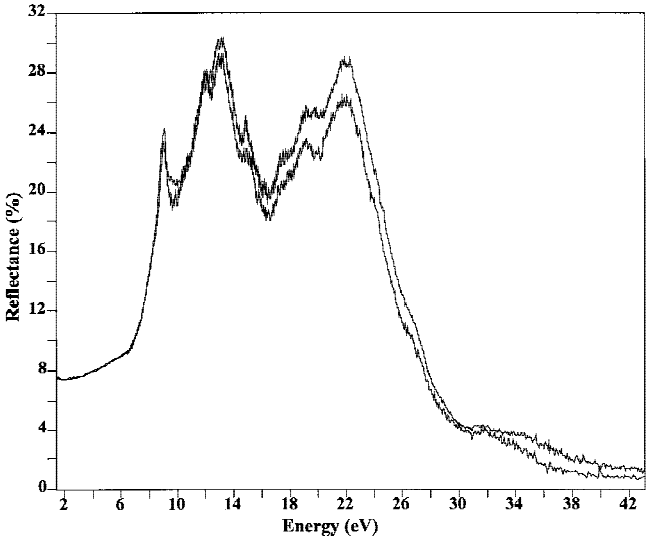

Fig. 1. Reflectance of single-crystal α-Al_2O_3, for E perpendicular to c-axis, determined using VUV and UV/visible spectroscopies.

The mean free path is 95.1 ± 0.4 nm for α-Al_2O_3 and 100.5 ± 0.2 nm for γ- and δ-Al_2O_3 by the index sum rule.[24] This is consistent with the previously published value of 112 ± 2 nm for α-Al_2O_3,[17] because, in that case, a smaller collection angle has been used, increasing the mean free path, because it depends on the range of acceptance angle.

(3) Comparison between VUV Spectroscopy and EELS

The data of Figs. 6 and 7 for energies up to 40 eV also are overlaid in Figs. 2 and 3, respectively, for more detailed comparison with the VUV spectroscopy results. The real part of the interband transition strength determined from EELS has a lower intensity for energies 12–22 eV, whereas it is roughly the average of the two VUV spectroscopy measurements for higher energies. All structures are sharper in the VUV-spectroscopy-determined result, as would be expected for the higher-energy

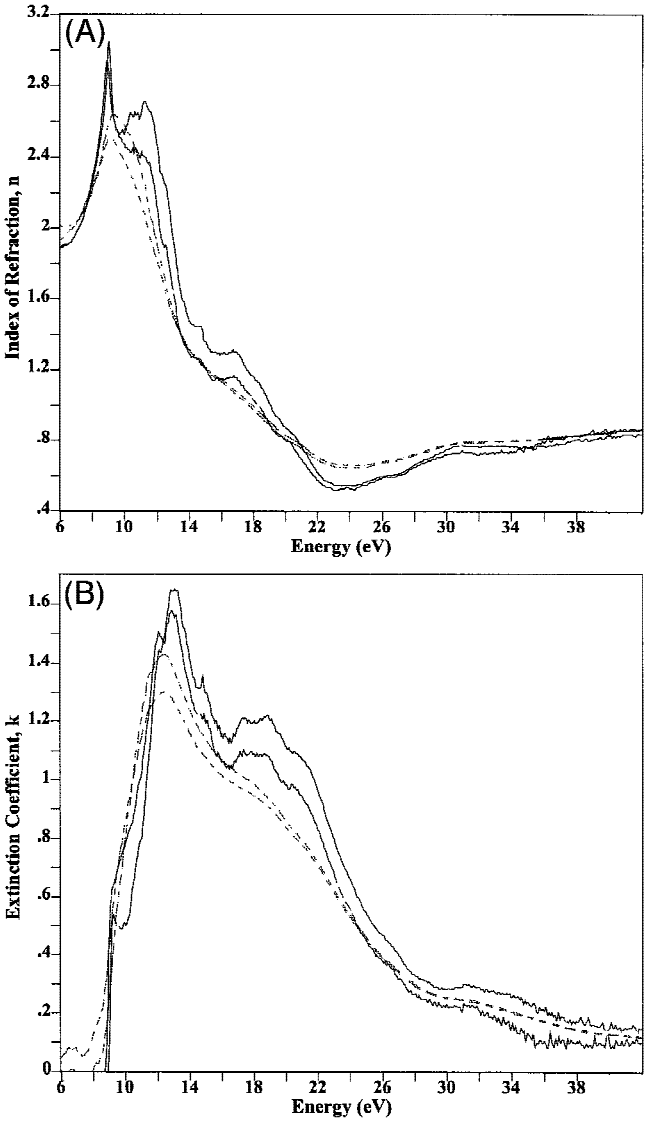

Fig. 3. Complex index of refraction ($n + ik$) consisting of (A) the index of refraction and (B) the extinction coefficient of single-crystal α-Al_2O_3, for E perpendicular to the c-axis, determined by KK analysis of VUV and UV/visible reflectance data. For comparison, the results from KK analysis of EELS data of α-Al_2O_3 also are shown (dashed lines).

resolution of VUV spectroscopy. The exciton also is not resolved in the EELS, or, at most, appears as a weak shoulder. Apart from this, the overall shapes are similar between both methods. For the complex part of the interband transition strength, again the difference between the sharpness of the features prevails, with overall agreement. The complex index of refraction has similar trends as the interband transition strength but is a less-sensitive variable in which to observe these subtle differences.

For further comparison, we have calculated the reflectance from the EELS results and have compared it with the measured VUV spectroscopy reflectance (Fig. 8). Again, VUV spectroscopy exhibits sharper features, with a big difference between 15 and 30 eV, the energy range where EELS spectra are dominated by the collective electron excitations of the plasmon oscillations. Otherwise, the absolute scale of both agree, and the EELS extends the energy range up to 140 eV. Furthermore, we have calculated the energy-loss function from the VUV spectroscopy results and have compared both of the energy-loss functions in Fig. 9. The VUV spectroscopy features are sharper, but this alone cannot explain the difference in the main peak at 26 eV. Also, for energies >35 eV, the VUV spectroscopy data exhibit a strong noise component, because the magnitude of the reflectance signal is very low ($R < 1\%$) and, therefore, difficult to measure accurately, whereas, in this range, the EELS spectra are relatively stronger.

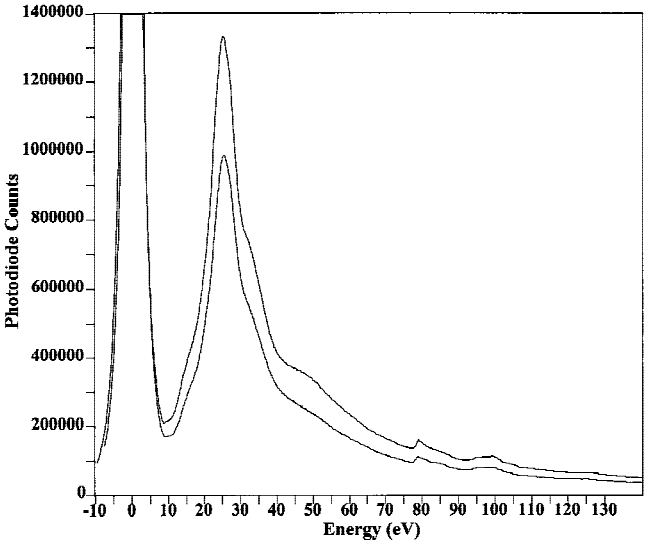

Fig. 4. Raw EELS spectra for thin-film α-Al_2O_3 measured using STEM. These spectra show the zero-loss peak (0 eV), the plasmon peak (26 eV), the effects of multiple scattering (~50 eV), and the aluminum L-edge (>78 eV).

(4) Other Al_2O_3 Phases

EELS data taken from both γ- and δ-Al_2O_3 have been analyzed in a manner similar to the data for α-Al_2O_3. The energy-loss functions (Fig. 10) for both phases agree well with each other and show differences with respect to α-Al_2O_3. These differences are more pronounced when viewed in the real part of the interband transition strength, Re[J_{cv}], (Fig. 11). Although γ- and δ-Al_2O_3 remain almost indistinguishable, α-Al_2O_3 has stronger transitions between 10 and 20 eV. Although α-Al_2O_3 has two prominent features at 30 and 50 eV, γ- and δ-Al_2O_3 have only one, centered at 40 eV. The intensity above 78 eV for the excitation of the aluminum L-shell electron is stronger, with sharper features for α-Al_2O_3. Compared to this, the differences in the index of refraction for all three phases (Fig. 12) are minor; only the maximum at 10 eV is significantly higher for the α-Al_2O_3.

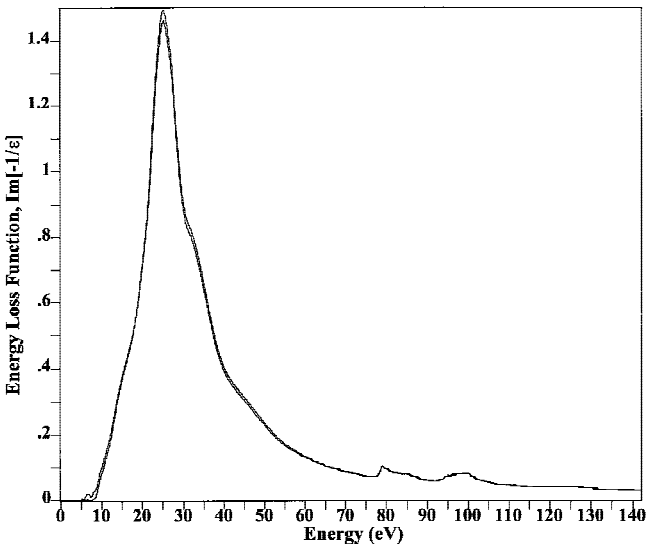

Fig. 5. Energy-loss functions for thin-film α-Al_2O_3 after single-scattering correction and zero-loss peak removal.

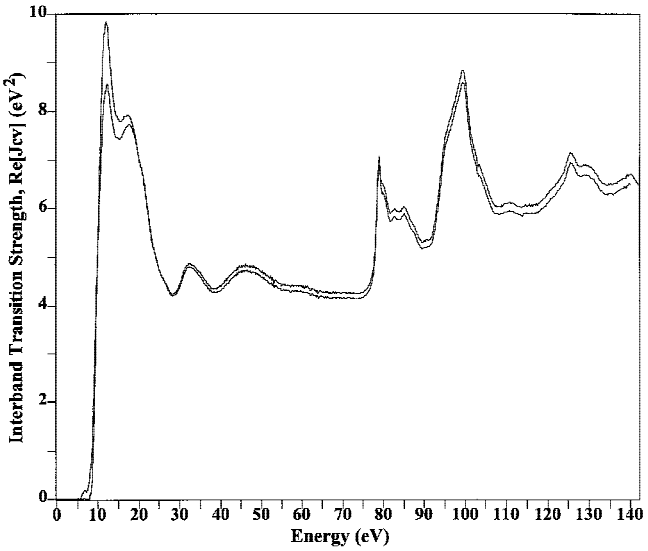

Fig. 6. Interband transition strength, Re(J_{cv}), of thin-film α-Al_2O_3, determined by KK analysis of EELS data.

V. Discussion

Here we discuss the two experimental methods and their performance followed by a comparison of the optical property results from both methods and a comparison to literature results.

(1) Reflectance

The differences in the results for the as-supplied and annealed single-crystal α-Al_2O_3 samples (Figs. 1–3) indicate the important effects resulting from the details of the specimen preparation. The sharper features for the annealed material result from annealing surface-polishing damage that reduces the level of exciton scattering and increases the prominence of the 9 eV peak.[35,36] Formally, surface reconstructions in Al_2O_3, which are expected at 1200° or 1300°C, are not expected to play a role, because, at these energies, absorption coefficients ($\alpha = 4\pi k/\lambda$) are of the order of 1×10^6 cm^{-1}, and, therefore, the reflectance originates from a surface layer of thickness 100 nm. Moreover, heat treatment at these temperatures is not expected to change the stoichiometry of Al_2O_3. The quality of both data sets is good and in agreement with each other, and only the direct comparison reveals the differences. Some of the differences might also result from slightly different splicing of the various energy regions in the data set, but these data do not involve extensive data manipulation in preparing the reflectance curves. Although both data sets then are analyzed identically, the differences in the interband transition strength are very pronounced. This is a manifestation of the fact that KK dispersion analysis and the transformations of the optical properties are integral transforms, so that small differences not visible in one optical variable in a particular energy range continue to produce dramatic and important differences in another optical property in that same energy range. This also means that different data sets might appear to be similar in some optical properties (here for the reflectance (Fig. 1)), and the complex index of refraction (Fig. 3), but pronounced differences in other properties (here for the interband transition strength (Fig. 2)). Another effect is that the exciton at 9 eV, which is clearly resolved in both reflectance data sets, is resolved only for the annealed material in the interband transition strength. This emphasizes the importance of studying the many different optical properties on an equal basis if one desires to understand the fundamental properties of a material.

(2) EELS

This discussion touches only briefly on the methods, because they have been analyzed extensively elsewhere.[6,17,28] Here the focus is on the reliability of the method and the information content.

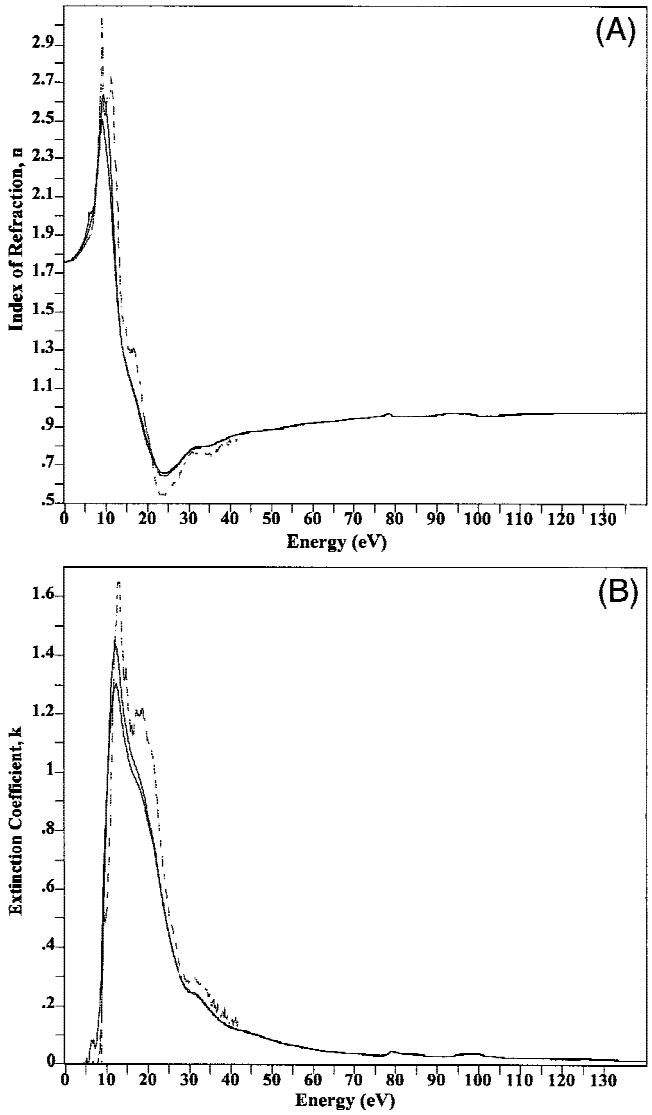

Fig. 7. Complex index of refraction ($n + ik$) consisting of (A) the index of refraction and (B) the extinction coefficient of thin-film α-Al_2O_3, determined by KK analysis of EELS data. Results from KK analysis of VUV data also are shown (dashed lines).

(A) Zero-Loss Extraction and Single-Scattering Deconvolution: The extraction of the zero-loss peak, including its wing, during the correction for multiple scattering, is the most critical step, whereas the actual correction for multiple scattering is reliable, because it relies only on the integrated intensity under the zero-loss peak, which is almost independent of the wing used. We have developed two methods[28] that give good results. The highest uncertainty is for the intensities just above the band gap, because the energy-loss function is small and the background from the zero-loss wing several times larger. The influence of this uncertainty on the optical properties can be estimated only from the results, because the integral transformations distribute it over all energies. The differences between the two data sets up to 20 eV (Figs. 2 and 6) may be due mainly to this uncertainty during zero-loss removal. Also, the apparent difference in the band gap (Fig. 2) also results from small differences in the zero-loss peak extraction. The only solution is to continue improving our extraction routines for the zero-loss peak, but the next steps in this are not immediately apparent. Unfortunately, the presence of the zero-loss peak is intrinsic to the method and cannot be avoided in an ~0 **q** momentum transfer measurement.

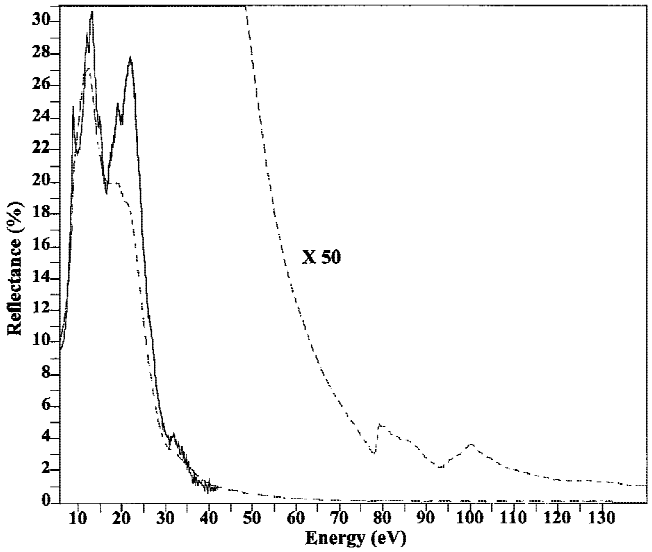

Fig. 8. Comparison of reflectance of α-Al_2O_3 between VUV and EELS (dashed line) data after KK analysis.

(B) KK Dispersion Analysis of EELS: KK dispersion analysis is long established. The only requirement is that the data go to zero at both sides, the band gap and the high energy. The former is automatically achieved during deconvolution. The latter is achieved through the high-energy wing, which is attached to the data before deconvolution to avoid truncation artifacts during FFT. Because the refractive indexes for α-, γ-, and δ-Al_2O_3 in the visible are well-known, the scaling of the energy-loss function poses no problem.

(C) Specimen Thickness and Surface Layers: The specimens are of uniform thickness in the investigated regions. Therefore, artifacts occurring during single-scattering deconvolution due to thickness variations can be excluded. The strong dependence on specimen thickness found for AlN has been attributed to the dissolution of oxygen in the material.[27] Such effects can be excluded here, because α-Al_2O_3 is known to exist only in its stoichiometric form.

The EELS spectrum also contains contributions from the specimen surface and surface layers. It is possible to extract these contributions, but it has been found that the influence on the result is negligible.[27]

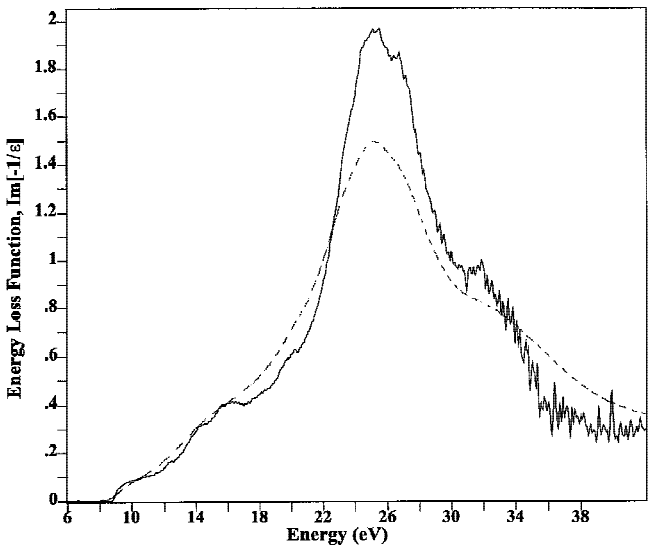

Fig. 9. Comparison of energy-loss functions of α-Al_2O_3 determined from KK analysis of VUV and EELS (dashed line) data.

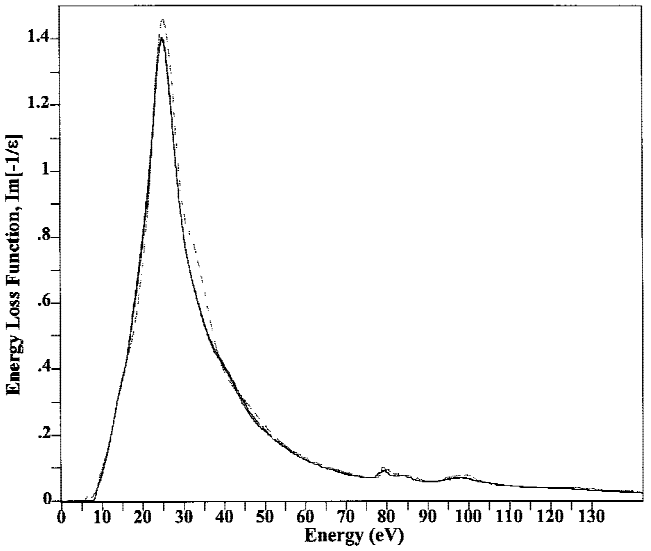

Fig. 10. Energy-loss functions from EELS data for thin-film γ- and δ-Al_2O_3 after single-scattering correction and zero-loss peak removal with results for α-Al_2O_3 (dashed line) shown for comparison.

(D) Reliability: The comparison of the data measured on two different regions of the specimen for α-Al_2O_3 (Figs. 2–7) shows close agreement in the energy-loss function (Figs. 4 and 5). The differences in the interband transition strength (Figs. 6 and 2) probably are due to the uncertainty of zero-loss removal (Section V(2)(A)). Therefore, the differences in the results can be attributed mainly to data analysis and not variations in the material. There is no criterion from which to choose one or the other data set. Therefore, the discrepancy between these represents a typical variation and leads to an uncertainty that cannot be avoided in the complex data analysis. Further improvements in the data acquisition and analysis can reduce this uncertainty but are not expected.

The differences between γ- and δ-Al_2O_3 are negligible in all optical properties, but they are significant as compared to α-Al_2O_3. As indicated above (Section II(2)(A)), a definite decision whether the analyzed phases are γ- and δ-Al_2O_3 cannot be made. Therefore, it might be that both analyzed spectra are from the same phase, which would explain the small differ-

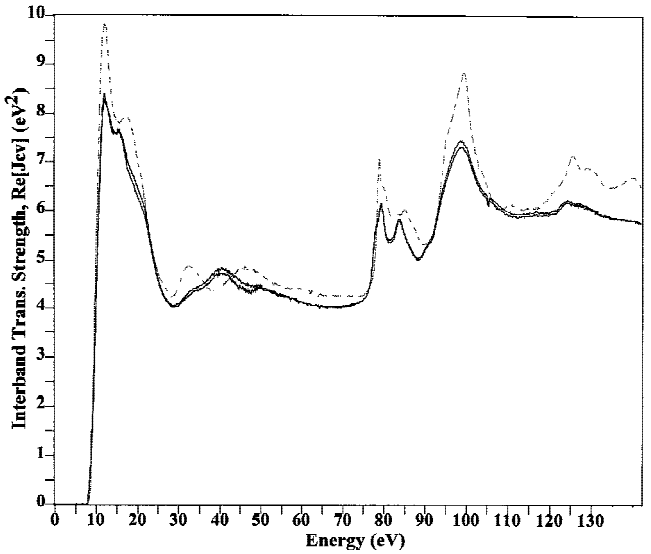

Fig. 11. Interband transition strength, Re(J_{cv}), of thin-film γ- and δ-Al_2O_3, determined by KK analysis of EELS data with results for α-Al_2O_3 (dashed line) shown for comparison.

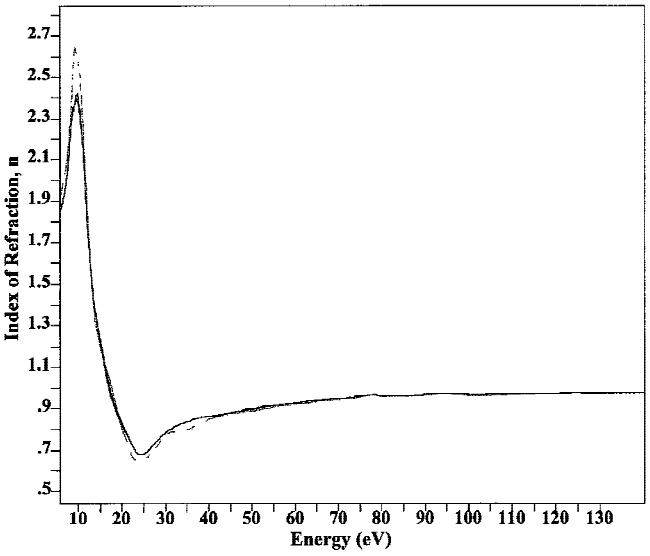

Fig. 12. Index of refraction, *n*, of thin-film γ- and δ-Al_2O_3, determined by KK analysis of EELS data with results for α-Al_2O_3 (dashed line) shown for comparison.

ences. Also, however, they are consistent if they are from the two different phases, because the main structure is identical, with only an ordering for the δ-Al_2O_3. This might have only a minor influence on the optical properties.

(3) Comparison of Methods

The same optical properties determined by both methods are compared in Figs. 2, 3, 8, and 9.

(A) VUV Spectroscopy and EELS: Accuracy and Information Content: The energy resolution of VUV spectroscopy is higher than for EELS, which explains the sharper features in J_{cv} (Fig. 2), the index of refraction (Fig. 3) and reflectance (Fig. 8), and the energy-loss function (Fig. 9). In particular, for energies up to 20 eV, VUV spectroscopy resolves more details than EELS. This is most pronounced near the band gap, where the exciton in the interband transition strength occurs, which appears in EELS as a weak shoulder at most. From 20 to 30 eV, the EELS spectrum typically is dominated by the plasmon peak, where ε_1 approaches zero, and, therefore, the relative accuracy of the EELS data to extract other optical properties is reduced, as shown in Fig. 2. At energies >30 eV, the reflectance amplitude decreases for VUV spectroscopy measurements, and the relative accuracy of the data gets smaller, indicated by the large noise component in this energy range (Figs. 2 and 9). EELS can determine the optical properties up to 140 eV in the current work, or even much higher energies if desired. In this energy regime, there are no extremely sharp features; therefore, the lower energy resolution of the EELS is not a limiting factor. Therefore, EELS can determine the optical properties for an energy range that is accessible only to optical spectroscopy with a synchrotron. Synchrotron light sources also offer the possibility to perform polarized-light measurements with high resolution, as done, for example, by Tomiki *et al.*,[13,14] but, to date, this opportunity has not been exploited extensively.

The differences between the data sets for each method are an indication of how reproducibly each material can be measured and analyzed. The agreement, on an absolute scale, of optical properties determined from completely different experimental and analytical methods is very satisfying, while the discrepancies between both methods remain larger than the variations within each method. This indicates uncertainties in the complex data analysis and in the intrinsic information content of each measurement and how accurately this information can be extracted. This demonstrates that the use of multiple methods provides a higher degree of knowledge. This also reveals the level of accuracy achieved, which is not usually visible when only a single method is used.

(B) Tomiki's VUV Spectroscopy Results: In the papers by Tomiki *et al.*,[13,14] optical constants are reported for α-Al_2O_3. They have used a synchrotron light source that provides polarized light up to 120 eV, permitting the determination of the anisotropy of the optical constants. There are noticeable differences between their results and the data presented here. The reflectivity of Tomiki *et al.* shows the same features as ours, but there are differences in the scale, in particular for the exciton at 9 eV, which they have measured to be 20%, and we have measured as 24% from VUV spectroscopy. Above 120 eV, Tomiki *et al.* have a significant reflectivity of 0.1%, whereas, from our EELS data, it is only 0.03%. Resulting from this, their energy-loss function at the plasmon peak is only 1.2 units high, whereas we find 2 units from VUV spectroscopy and 1.5 units from EELS. Tomiki *et al.* have used the oscillator strength sum rule for the number of effective electrons as a criterion to assess the quality of their data. Although expecting 48 electrons up to the aluminum *L*-edge at 78 eV, they find 66 ± 2 from their data. Tomiki *et al.* mention that this number probably is even larger, considering the transitions at higher energies. This is explained as resulting from negative contributions to the sum rule at higher energies. This explanation may be correct, except that it requires large negative contributions to the sum rule. It appears that this large sum rule discrepancy occurs because of the larger values of ε_2 (or the energy-loss function) at energies >70 eV, which are about twice our values. This is not apparent in the calculation of ε_∞, because ε_2 is divided by *E*, whereas, for N_{eff}, it is multiplied by *E*. Therefore, the agreement in one sum rule does not prove the quality of the data decisively, but, rather, numerous sum rules should be considered.[35]

We have evaluated the oscillator strength sum rule for our data (Fig. 13) using volumes per Al_2O_3 formula, given in Table I. For each formula unit of Al_2O_3, there are 24 valence electrons, 16 more electrons in the aluminum *L*-shell, 6 in the oxygen *K*-shell, and 4 in the aluminum *K*-shell. The edges for the latter two are not included in our data. From our VUV spectroscopy and EELS data for α-Al_2O_3, we find 16.8 electrons, including transitions up to 42 eV, and 21.7 electrons for all transition up to 78 eV from the EELS measurement. This is smaller than the 24 valence electrons expected in Al_2O_3, but there are transitions from the valence band with energies >78 eV. Integrating up to 140 eV, we find 28 electrons from our

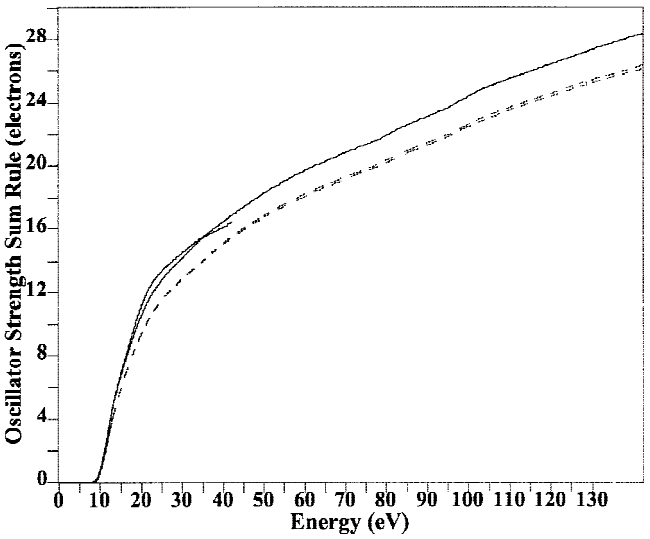

Fig. 13. Oscillator strength sum rules for three phases of Al_2O_3, calculated on an Al_2O_3 formula-unit basis. Sum rules for α-Al_2O_3 from both VUV and EELS data (solid lines) and thin-film γ- and δ-Al_2O_3 (dashed lines) are shown.

EELS data. This again is smaller than the total number of electrons in the valence band and the aluminum *L*-shell (40 electrons expected), but there are many more transitions of these electrons at higher energies. Because of this better consistency with the sum rule, we believe that the absolute values of the optical properties presented in this paper for energies >50 eV are more reliable than the previous results of Tomiki *et al.*[13,14] These types of disagreements in the magnitudes of the optical constants can result from the details of the KK dispersion analysis, because these transforms determine the magnitudes at all energies.

For γ- and δ-Al_2O_3, the sum rule gives slightly smaller values per Al_2O_3 formula unit than for α-Al_2O_3. For the valence region, up to 42 eV, we find 15.5 electrons, with 20 electrons observed up to 78 eV and 26.2 electrons observed up to 140 eV.

VI. Conclusion

The determination of optical properties remains a challenging task, despite the advanced methods of data acquisition and analysis. Minor variations in the specimen preparation, the data acquisition, or the data analysis may lead to pronounced differences visible in certain optical properties while other optical properties may not emphasize these subtleties. Because of the complex relationship between all the optical constants, it is impossible to predict the influence on one particular variation in the specimen, data, or analysis on the results. The comparison of various data sets, carefully analyzed, seems to be the only way to obtain an indication of the uncertainty in the information content of the final results. These sensitivities of the different optical properties and the experimental methods also demonstrate how, for some problems, one method is intrinsically more accurate in one energy range, and the differences are seen most prominently in one of the optical properties. VUV spectroscopy measurements have better energy resolution but are limited to energies <40 eV. EELS gives access to all energies but resolves fewer features and is particularly uncertain for energies just above the band gap. For an unbiased sense of the accuracy and variability of our knowledge of the optical properties, multispecimen and multimethod studies are essential. Future developments should reduce the uncertainties and the discrepancies between the methods, which leads to more confidence in the optical constants determined.

Acknowledgments: We thank Dipl. Phys. A. Dorneich, Dr. S. Loughin, and Professor M. Rühle for discussions and I. Levin for provision of the TEM samples. One of us (HM) acknowledges financial support from the Volkswagen Stiftung under Contract No. I/70 082.

References

[1]I. H. Malitson and M. J. Dodge, ''Refractive Index and Birefringence of Synthetic Sapphire,'' *J. Opt. Soc. Am.*, **62**, 1405 (1972).

[2]H.-J. Hagemann, W. Gudat, and C. Kunz, ''Optical Constants from the Far Infrared to the X-ray Region: Mg, Al, Cu, Ag, Au, Bi, C, and Al_2O_3,'' *J. Opt. Soc. Am.*, **65**, 742–44 (1975).

[3]M. E. Innocenzi, R. T. Swimm, M. Bass, R. H. French, A. B. Villaverde, and M. R. Kokta, ''Room-Temperature Optical Absorption in Undoped α-Al_2O_3,'' *J. Appl. Phys.*, **67** [12] 7542–46 (1990).

[4]M. E. Thomas, W. J. Tropf, and S. L. Gilbert, ''Vacuum-Ultraviolet Characterization of Sapphire, AlON, and Spinel Near the Band Gap,'' *Opt. Eng.*, **32**, 1340–43 (1993).

[5]R. H. French, R. M. Cannon, L. K. DeNoyer, and Y.-M. Chiang, ''Full Spectral Calculation of Non-Retarded Hamaker Constants for Ceramic Systems from Interband Transition Strengths,'' *Solid State Ionics*, **75**, 13–33 (1995).

[6]R. H. French, H. M. Müllejans, D. J. Jones, G. Duscher, R. M. Cannon, and M. Rühle, ''Dispersion Forces and Hamaker Constants for Intergranular Films in Silicon Nitride from Spatially Resolved–Valence Electron Energy Loss Spectrum Imaging,'' *Acta Materialia*, **46** [7] 2271–87 (1998).

[7]H. D. Ackler, R. H. French, and Y.-M. Chiang, ''Comparison of Hamaker Constants for Ceramic Systems with Intervening Vacuum or Water: From Force Laws and Physical Properties,'' *J. Colloid Interface Sci.*, **179**, 460–69 (1996).

[8]C. Argento and R. H. French, ''Parametric Tip Model and Force–Distance Relation for Hamaker Constant Determination from AFM,'' *J. Appl. Phys.*, **80**, 6081–90 (1996).

[9]R. H. French, ''Electronic Structure of α-Al_2O_3, with Comparison to AlON and AlN,'' *J. Am. Ceram. Soc.*, **73** [3] 477–89 (1990).

[10]M. L. Bortz, R. H. French, D. J. Jones, R. V. Kasowski, and F. S. Ohuchi, ''Temperature Dependence of the Electronic Structure of Al_2O_3, $MgAl_2O_4$, and MgO,'' *Phys. Scr.*, **41** [4] 537–41 (1990).

[11]R. H. French, R. L. Coble, R. V. Kasowski, and F. S. Ohuchi, ''Vacuum-Ultraviolet, Photoemission, and Theoretical Studies of the Electronic Structure of Al_2O_3 up to 1000°C,'' *Physica B* (*Amsterdam*), **150** [1–2] 47–49 (1988).

[12]R. H. French, D. J. Jones, and S. Loughin, ''Interband Electronic Structure of α-Al_2O_3 up to 2167 K,'' *J. Am. Ceram. Soc.*, **77**, 412–22 (1994).

[13]T. Tomiki, Y. Ganaha, T. Shikenbaru, T. Futemma, M. Yuri, Y. Aiura, S. Sato, H. Fukutani, H. Kato, T. Miyahara, A. Yonesu, and J. Tamashiro, ''Anisotropic Optical Spectra of α-Al_2O_3 Single Crystals in the Vacuum-Ultraviolet Region. I. Spectra of Absorption Tail and Reflectivity,'' *J. Phys. Soc. Jpn.*, **62** [2] 573–84 (1993).

[14]T. Tomiki, Y. Ganaha, T. Futemma, T. Shikenbaru, Y. Aiura, M. Yuri, S. Sato, H. Fukutani, H. Kato, T. Miyahara, J. Tamashiro, and A. Yonesu, ''Anisotropic Optical Spectra of α-Al_2O_3 Single Crystals in the Vacuum-Ultraviolet Region. II. Spectra of Optical Constants,'' *J. Phys. Soc. Jpn.*, **62** [4] 1372–87 (1993).

[15]F. Gervais, ''Aluminum Oxide (Al_2O_3)''; pp. 761–75 in *Handbook of Optical Constants of Solids II*. Edited by E. D. Palik. Academic Press, New York, 1991.

[16]W. J. Tropf and M. E. Thomas, ''Aluminum Oxide (Al_2O_3) Revisited''; pp. 653–82 in *Handbook of Optical Constants of Solids*, Vol. III. Edited by E. D. Palik. Academic Press, New York, 1997.

[17]H. Müllejans and R. H. French, ''Interband Electronic Structure of a Near Σ11 Grain Boundary in α-Alumina Determined by Spatially Resolved Valence Electron Energy-Loss Spectroscopy,'' *J. Phys. D: Appl. Phys.*, **29**, 1751–60 (1996).

[18]S.-D. Mo, W. Y. Ching, and R. H. French, ''Electronic Structure of a Near Σ11 *a*-Axis Tilt Grain Boundary in α-Al_2O_3,'' *J. Am. Ceram. Soc.*, **79**, 627–33 (1996).

[19]S.-D. Mo, W. Y. Ching, and R. H. French, ''Optical Properties of a Near Σ11 *a*-Axis Tilt Grain Boundary in α-Al_2O_3,'' *J. Phys. D: Appl. Phys.*, **29**, 1761–66 (1996).

[20]I. Levin, L. A. Bendersky, D. G. Brandon, and M. Rühle, ''Cubic to Monoclinic Phase Transformations in Alumina,'' *Acta Materialia*, **45** [9] 3659–69 (1997).

[21]R. H. French and J. B. Blum, ''Electronic Structure and Conductivity of Al_2O_3''; pp. 111–34 in Ceramic Transactions, Vol. 7, *Sintering of Advanced Ceramics*. Edited by C. A. Handwerker, J. E. Blendell, and W. Kaysser. American Ceramic Society, Westerville, OH, 1990.

[22]R. H. French, ''Laser-Plasma Sourced, Temperature-Dependent VUV Spectrophotometer Using Dispersive Analysis,'' *Phys. Scr.*, **41** [4] 404–408 (1990).

[23]M. L. Bortz and R. H. French, ''Optical Reflectivity Measurements Using a Laser Plasma Light Source,'' *Appl. Phys. Lett.*, **55** [19] 1955–57 (1989).

[24]R. F. Egerton, *Electron Energy-Loss Spectroscopy in the Electron Microscope*, 2nd ed. Plenum, New York, 1996.

[25](a)R. de L. Kronig, ''On The Theory of Dispersion of X-rays,'' *J. Opt. Soc. Am.*, **12**, 547–57 (1926). (b)C. J. Gorter and R. de L. Kronig, ''On the Theory of Absorption and Dispersion in Paramagnetic and Dielectric Media,'' *Physica III*, **9**, 1009–20 (1936).

[26]H. A. Kramers, ''La Diffusion de la Lumière par les Atomes,'' *Atti. Congr. Int. Fis. Como.*, **2**, 545–57 (1927).

[27]D. J. Jones, R. H. French, S. Loughin, A. D. Dorneich, H. Müllejans, and P. F. Carcia, ''Optical Properties of Aluminum Nitride Determined from Vacuum-Ultraviolet Spectroscopy and Spectroscopic Ellipsometry,'' unpublished work.

[28]A. D. Dorneich, R. H. French, H. Müllejans, S. Loughin, and M. Rühle, ''Quantitative Analysis of Valence Electron Energy-Loss Spectra of Aluminum Nitride,'' *J. Microsc.*, **191** [3] 286–96 (1998).

[29]P. Schattschneider, *Fundamentals of Inelastic Electron Scattering*. Springer, Wien, Austria, 1986.

[30]M. L. Bortz and R. H. French, ''Quantitative, FFT-Based, Kramers Kronig Analysis for Reflectance Data,'' *Appl. Spectrosc.*, **43** [8] 1498–501 (1989).

[31]W. Sellmeier, ''II. Regarding the Sympathetic Oscillations Excited in Particles by Oscillations of the Ether and Their Feedback to the Latter, Particularly as a Means of Explaining Dispersion and Its Anomalies'' (in Ger.), *Ann. Phys. Chem.*, **147**, 525–54 (1872).

[32]F. Wooten, *Optical Properties of Solids*, Academic Press, New York, 1972.

[33]Table: ''Physical Constants of Inorganic Compounds,'' *Handbook of Chemistry and Physics*, 53rd ed., p. B-64. CRC Press, Boca Raton, FL, 1972.

[34]D. Y. Smith, ''Dispersion Theory, Sum Rules, and Their Application to the Analysis of Optical Data''; p. 35–68 in *Handbook of Optical Constants of Solids*. Edited by E. D. Palik. Academic Press, New York, 1985.

[35]Y. Toyozawa, ''Theory of Line-Shapes of the Exciton Absorption Bands,'' *Prog. Theor. Phys.*, **20** [1] 53–81 (1958).

[36]M. Skibowski, G. Sprussel, and V. Saile, ''Fine Structure and Temperature Dependence of Shallow Core Excitons in Insulators and Semiconductors,'' *Appl. Opt.*, **19** [23] 3978–86 (1980). □